# Voxel-wise assessment of lung aeration changes on CT images using image registration: application to acute respiratory distress syndrome (ARDS)

Maciej Orkisz, Alfredo Morales Pinzon, Jean-Christophe Richard, Claude Guérin, Leslie Evelyn Solórzano Vargas, Daniela Florentina Sicaru, Camila García Hernández, Margarita Gómez Ballén, Bruno Neyran, Eduardo E. Dávila Serrano, et al.

**International Journal of Computer Assisted Radiology and Surgery manuscript No.**
(will be inserted by the editor)

# Voxel-wise assessment of lung-aeration changes on CT images using image registration: Application to acute respiratory distress syndrome (ARDS)

**Maciej Orkisz · Alfredo Morales Pinzón · Jean-Christophe Richard · Claude Guérin · Leslie Evelyn Solórzano Vargas · Daniela Sicaru · Camila García Hernández · Margarita M. Gómez Ballén · Bruno Neyran · Eduardo E. Dávila Serrano · Marcela Hernández Hoyos**

Received: date / Accepted: date

**Abstract** *Purpose*: 1) To improve the accuracy of global and regional alveolar-recruitment quantification in CT-scan pairs by accounting for lung-tissue displacements and deformation, 2) To propose a method for local-recruitment calculation. *Methods*: Recruitment was calculated by subtracting the quantity of non-aerated lung tissues between expiration and inspiration. To assess global recruitment, lung boundaries were first interactively delineated at inspiration, then they were warped based on automatic image registration to define the boundaries at expiration. To calculate regional recruitment, the lung mask defined at inspiration was cut into pieces and these were also warped to encompass the same tissues at expiration. Local-recruitment map was calculated as follows: for each voxel at expiration, the matching location at inspiration was determined by image registration, non-

This work was performed within the framework of the LABEX PRIMES (ANR-11-LABX-0063) of Université de Lyon, within the program "Investissements d'Avenir" (ANR-11-IDEX-0007) and supported by the French-Colombian program ECOS-Nord, project C15M04.

M. Orkisz · A. Morales Pinzón · J.-C. Richard · L. E. Solórzano Vargas · D. Sicaru · E. E. Dávila Serrano · B. Neyran
Univ Lyon, Université Claude Bernard Lyon 1, INSA-Lyon, UJM-Saint Etienne, CNRS, Inserm, CREATIS UMR 5220, U1206, F-69621, Villeurbanne, France
E-mail: maciej.orkisz@univ-lyon1.fr

A. Morales Pinzón · L. E. Solórzano Vargas · C. García Hernández · M. M. Gómez Ballén · M. Hernández Hoyos
Systems and Computing Engineering, Universidad de los Andes, Bogotá, Colombia

J.-C. Richard · C. Guérin
Service de Réanimation Médicale, Hôpital de la Croix Rousse, Hospices Civils de Lyon, France

C. Guérin
Université de Lyon, Université Lyon 1, Lyon, France; IMRB, INSERM 955Eq13, Créteil, France; HP2 INSERM 1042, Grenoble, France; Service de médecine intensive réanimation, CHU Grenoble-Alpes, Grenoble, France

D. Sicaru
Faculty of Electronics, Telecommunications and Information Technology, University Politehnica of Bucharest, Romania

aerated voxels were counted in the neighborhood of the respective locations, and the voxel-count difference was normalized by the neighborhood size. The methods were evaluated on 120 image pairs of twelve pigs with experimental acute respiratory distress syndrome. *Results*: The dispersion of global- and regional-recruitment values decreased when using image registration, compared to the conventional approach neglecting tissue motion. Local-recruitment maps overlaid onto the original images were visually consistent, and the sum of these values over the whole lungs was very close to the global-recruitment estimate, except four outliers. *Conclusions*: Image-registration can compensate lung-tissue displacements and deformation, thus improving the quantification of alveolar recruitment. Local-recruitment calculation can also benefit from image registration, and its values can be overlaid onto the original image to display a local-recruitment map. They also can be integrated over arbitrarily-shaped regions to assess regional or global recruitment.

**Keywords** Acute Respiratory Distress Syndrome · Alveolar recruitment · Computed Tomography · Image processing · Image registration

## 1 Introduction

Acute respiratory distress syndrome (ARDS) is a severe pathological condition entailing mortality rates as high as 40% [9]. The syndrome is clinically characterized by a mixture of alveolar collapse, edema, and inflammation, leading to a dramatic drop in oxygenation, while its radiological hallmark is the presence of diffuse opacities within the lungs. ARDS may originate from various aggressions of the lungs, e.g., mechanical trauma, aspiration of chemicals, or pneumonia. Despite emergence of promising therapeutic alternatives [3], mechanical ventilation is generally used to maintain the patient's gas exchanges during the treatment of the syndrome's cause. Two main ventilator parameters, positive end-expiratory pressure (PEEP) and tidal volume (Vt), should ideally be set so as to guarantee sufficient gas exchanges, namely by recruiting collapsed alveoli, i.e., reopening and maintaining them open, while avoiding harmful phenomena, such as overdistention of already aerated tissues and cyclic alveolar reopening-closing [9]. The choice of the best PEEP and Vt values requires assessing patient's lung aeration in response to distinct settings and, in particular, quantifying the recruitment.

Lung aeration can be assessed using computed-tomography (CT) images and the relationship between CT numbers (Hounsfield units – HU) and tissue-to-air ratio in each voxel [4]. According to their CT number, ranging from −1000 to 100 HU, the voxels within the lungs are classified as over-inflated, normally-, poorly-, or non-aerated [15,4]. Using the latter class (−100 to 100 HU), Gattinoni et al. [5] have proposed to calculate the recruitment as the difference in quantity of non-aerated pulmonary tissue between distinct ventilation conditions. These conditions may relate to different end-expiratory pressures (typically, zero – ZEEP – and positive – PEEP) or to end-exhale and end-inhale ventilator pauses, and the corresponding recruitment is referred to as PEEP-induced or intratidal, respectively. Calculating the recruitment according to this method requires delineating the lungs in the image pair acquired in the conditions of interest (ZEEP-PEEP or exhale-inhale) followed by counting the non-aerated voxels in the segmented lungs. This method is conceptually well suited to assess the recruitment globally,

in the whole lung, but it has also been used in a more localized manner: 1) as lung segmentation was performed manually, which is very tedious and time consuming, the quantification often was restricted to one slice [2,10], 2) as assessing the recruitment more locally is of great interest, the segmented slices sometimes have been subdivided into several intervals along the antero-posterior direction [5, 2,10], and 3-dimensional (3D) volumes have undergone both antero-posterior and cranio-caudal subdivision [1].

Unfortunately, such regional quantification may be adversely affected by the pulmonary-tissue motion. Indeed, while the global quantification treats the lung as a whole and thus compares the same tissues, an isolated slice or arbitrarily-shaped region is rather unlikely to contain exactly the same tissues in the two compared images, unless special precautions are taken to carefully align the image contents. Although attempts to perform such an alignment were made, e.g., by selecting a slice located at constant distance above the diaphragm dome [4], these can compensate only for translational movements, while the actual motion patterns of the pulmonary tissues may be much more complex [9]. This might explain some previously reported inconsistencies, namely, negative recruitment values observed despite increased PEEP [5,2]. To the best of our knowledge, only one work accounted for non-rigid tissue motion by manually delineating the region of interest in both compared CT scans, using a specific threshold-based display and perceptible landmarks [7]. In the work presented in this article, 3D alignment of the tissues was performed automatically, using a standard image-registration algorithm, so as to reduce the operator's workload associated with manual delineation, similarly to [8,16], and to make sure that the same regions were compared in the two images despite complex displacements of the tissues. Benefits of this automatic alignment to assess regional recruitment will be demonstrated on large parallelepiped regions. Advantages and drawbacks of more localized quantification, using smaller regions, will be discussed, leading to a proposal of a fully-local quantification method capable of displaying a recruitment map at voxel-size resolution.

## 2 Materials and Methods

After describing the data (Section 2.1) and summarizing the method used to align the tissues (Section 2.2) we will introduce our main contribution in the second part of Section 2.3, followed by a description of the experimental work (Section 2.4). Without loss of generality, we will focus on intratidal recruitment, and the notations $I_1$ and $I_2$ will respectively stand for images acquired at end-exhale and end-inhale ventilator pauses (also referred to as *expi* and *inspi*).

### 2.1 Data sets

In this work, we have used 120 3D-CT image pairs from a previous study [11, 8] representing twelve mechanically-ventilated pigs (constant $Vt = 6\,\mathrm{ml/kg}$) with experimental ARDS. Their in-plane resolution ranged from $0.46 \times 0.46$ to $0.59 \times 0.59\,\mathrm{mm}^2$ (matrix size $512 \times 512$), and the slice spacing from 0.70 to 1.00 mm (306 to 503 slices per CT image). For each pig, ten image pairs were acquired at end-exhale and end-inhale ventilator pauses with distinct PEEP values evenly

decreasing from 20 to 2 cm $H_2O$. Segmentation results were interactively obtained by a medical expert who traced contours using TurtleSeg[1] software [14,13].

## 2.2 Image registration

Prior to quantifying the aeration, image pairs corresponding to the same PEEP were aligned in view of calculating intratidal recruitment. A conventional non-rigid registration process was implemented in `elastix` framework [6,12] with the following settings: B-Spline transformation and interpolator, adaptive stochastic gradient descent with a maximum of 2000 iterations, normalized-mutual-information distance function, and a four-level multi-resolution scheme. *Expi* images were used as fixed and *inspi* images were moving. For each image pair, the transformation $\mathcal{T}$ resulting from the image-registration process was used to warp the lung mask delineated in one image (moving image), or its sub-regions, and thereby obtain the corresponding lung (or sub-region) mask(s) in the other image (fixed image).

## 2.3 Aeration quantification

In this section we will first elaborate on the regional assessment of the recruitment, with the focus on parallelepiped regions, and then we will explain how the seminal method can be extended to regions as small as one voxel.

### *2.3.1 Regional recruitment*

According to the seminal method [5], lung recruitment can be calculated by first counting the non-aerated voxels (-100 to 100 HU) separately within lung masks segmented in $I_1$ and $I_2$, then subtracting the respective counts: $r = n_1 - n_2$. Actually, the calculated recruitment is usually expressed in grams. To this purpose, the voxel-count difference is multiplied by the voxel volume and by air-free lung-tissue density that is usually assumed to be 1 g/ml. The same method was applied regionally [1] in order to assess the recruitment differences in the antero-posterior direction and at different heights. As ARDS manifestations often are heterogeneously distributed throughout the lungs, this approach may be generalized to also assess the differences in the remaining direction (from left to right), by cutting the lungs into "parallelepiped" regions that will be referred to as "boxes".

Assuming that the lungs were already segmented, our boxes can be defined by taking the bounding-box of the segmented lungs and cutting it with orthogonal planes. This is illustrated by Figure 1 (left), where one plane grossly separates the left and right lungs, another plane separates the anterior and posterior regions, and two horizontal planes arbitrarily separate top, middle, and bottom regions of equal height. When both images ($I_1$ and $I_2$) are cut into boxes, box pairs $\mathbf{B}_{1l}$ and $\mathbf{B}_{2l}$ thereby defined (where the common index $l$ refers to the same location in the respective images) are likely not to represent the same tissues, because the deformation of the lungs observed between these images generally cannot be fully represented by a simple transformation preserving the shape of the boxes. We

[1] `http://www.turtleseg.org/`

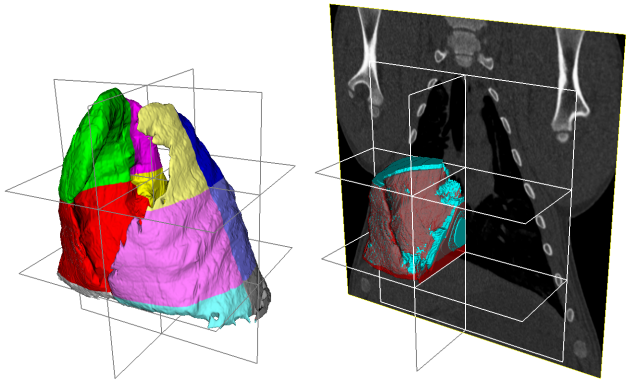

**Fig. 1** "Parallelepiped" regions. (*Left*) Lungs segmented in $I_2$ image and cut into big boxes. (*Right*) Example region displayed in its initial position in $I_2$ (red) and warped with use of image registration to encompass the same tissues in $I_1$ (cyan): color differences highlight non-overlapping parts that would give rise to inconsistent recruitment values if those were calculated by conventional approaches (without image registration).

propose to overcome this problem by use of image registration: the boxes in $I_2$ still are defined by orthogonal planes, but their corresponding regions in $I_1$ are warped according to the transformation obtained in the registration process (Fig. 1 right).

Smaller regions may be obtained using more planes, thereby permitting a more and more local assessment of the recruitment. Nevertheless, counting voxels in a box as small as one voxel makes no sense and would require a perfect voxel-to-voxel alignment, which cannot be achieved in practice by image registration techniques. We propose, therefore, a different approach devised to compute local recruitment with voxel-size resolution, while using a sufficiently large support thereby restricting the sensitivity to registration uncertainties and to noise.

### *2.3.2 Local recruitment*

In the proposed method, each voxel within the segmented lungs $\mathcal{L}$ is assigned a recruitment value calculated in a finite-size sliding box similarly to conventional filtering in image processing. To illustrate this proposal, let us consider:

- a voxel $\mathbf{v} \in \mathcal{L}_1$ located in the fixed image $I_1$ at a position $\mathbf{x}$,
- a transformation $\mathcal{T}$ resulting from image registration and projecting the fixed image $I_1$ onto the moving image $I_2$,
- a vector $\mathbf{t}$ deduced from $\mathcal{T}$ and projecting $\mathbf{v}$ onto the corresponding voxel $\mathbf{v}'$ in $I_2$, such that the location of $\mathbf{v}'$ is $\mathbf{x}' = \mathbf{x} + \mathbf{t}$,
- a cube-shaped $S \times S \times S$-size box $\mathbf{B}'$ centered in $\mathbf{x}'$,
- and the corresponding box $\mathbf{B}$ centered in $\mathbf{x}$.

First, non-aerated voxels are separately counted in $\mathbf{B}$ and $\mathbf{B}'$. Then, the corresponding recruitment value is deduced from the respective counts $n$ and $n'$: $r = n - n'$. Eventually, this value is normalized by the box size and the result thus obtained, $\rho = r/S^3$, representing the ratio of recruited voxels in the considered box, is assigned to the voxel $\mathbf{v}$ in the recruitment map. The values of $\rho$ may range from 1 (when 100% of voxels within $\mathbf{B}$ are recruited) to $-1$ (100% derecruitment). The same procedure is repeated for each voxel $\mathbf{v} \in \mathcal{L}_1$.

### 2.4 Experiments

The details of each experiment are described hereafter and their main characteristics are summarized in Table 1.

*Experiment 1.* **Global** recruitment (in entire lungs) was assessed using two strategies, referred to as **a** and **b**. In **a** strategy, image registration was not used: lung masks $\mathcal{L}_1$ and $\mathcal{L}_2$ were obtained by interactive segmentation of *expi* and *inspi* images separately, like in previous work [1,2,4,10]. In **b** strategy, interactive delineation of the lung mask ($\mathcal{L}_2$) was performed only in the moving (*inspi*) image, while the mask $\mathcal{L}_1$ in the fixed (*expi*) image was obtained by using $\mathcal{T}$ to warp $\mathcal{L}_2$, because opacities observed at end-exhale are larger (more derecruited tissues), so contrasts are decreased, making the segmentation more difficult.

*Experiment 2.* **Regional** recruitment was calculated using twelve **big boxes** (Fig. 1) and the approaches described in Section 2.3.1, respectively referred to as **c** and **d**. Both approaches used the same strategy (**b** from the previous experiment) to obtain the external boundaries of the lung mask $\mathcal{L}_1$ (*expi*) from $\mathcal{L}_2$ (*inspi*), but they differed in the definition of the frontiers between the regions. In **c** approach, the bounding-box of each mask ($\mathcal{L}_1$ and $\mathcal{L}_2$) was separately cut by parallel and orthogonal planes. Please note, that this approach accounts for rigid displacements of the tissues, but not for more complex motion. In **d** approach, the boxes were parallelepiped only in the moving (*inspi*) image, while in the fixed (*expi*) image their frontiers were warped by the transformation $\mathcal{T}$.

*Experiment 3.* The same experiment (**regional** recruitment with approaches **c** and **d**) was repeated twice, with smaller boxes: $S \approx 5\,\text{cm}$ and $S \approx 1.5\,\text{cm}$, respectively referred to as **medium** and **small**. The values of $S$ are approximate, as the regions were obtained by cutting the bounding-box of the lungs with a constant number of equidistant planes, so the actual size $S$ was dependent on the lung size, which slightly varied between pigs and from one ventilation condition to another.

*Experiment 4.* Local recruitment was computed with box size comprised between $S \approx 0.3$ and the small-box size from the previous experiment. In this article, results obtained with box sizes of $S \approx 0.5$ and $S \approx 1.0\,\text{cm}$ will be reported to illustrate the observed tendencies. The actual value of $S$ was here independent of the lung size, but it was dependent on image resolution, because the actual size was calculated as the integer number closest to the preset size in millimeters.

**Table 1** Main characteristics of the experiments

| Experiment | 1 | 2 | 3 | 4 |
|---|---|---|---|---|
| Scope | global | regional | regional | local |
| Box size | whole lung | big: $S \approx 10\,\text{cm}$ | medium: $S \approx 5\,\text{cm}$<br>small: $S \approx 1.5\,\text{cm}$ | $S \approx 1.0\,\text{cm}$<br>$S \approx 0.5\,\text{cm}$ |
| Variants | **a**: no registration; $I_1$ & $I_2$ segmented independently<br>**b**: $I_2$ segmented; registration to infer lung mask in $I_1$ | **c**: no box warping; $\mathcal{L}_1$ & $\mathcal{L}_2$ cut independently<br>**d**: $\mathcal{L}_2$ cut using planes; warped boxes in $\mathcal{L}_1$ | **c**: no box warping; $\mathcal{L}_1$ & $\mathcal{L}_2$ cut independently<br>**d**: $\mathcal{L}_2$ cut using planes; warped boxes in $\mathcal{L}_1$ | |

### 2.5 Evaluation

CT remains the most accurate technique to measure tissue aeration *in vivo*, so no other technique could be used as reference. Additionally, as confirmed by our results, assessing the aeration from fully manual 3D segmentation of CT images is not reproducible enough to be used as independent standard. In the absence of ground truth, we mainly evaluated the consistency of the experimental points representing the recruitment vs. PEEP, calculated with distinct methods. For this purpose, dispersion of the experimental points was assessed. Primarily, two-factor analysis of variance (two-way ANOVA) was performed separately for each strategy, the two respective factors being the PEEP value and the pig. For each factor, we focused on the ratio between the variance $\sigma_f^2$ explained by this factor and the residual variance $\sigma_r^2$: $F = \sigma_f^2/\sigma_r^2$. This ratio is greater for the strategy leading to a smaller residual variance (unexplained by the variations of the factors).

Additionally, as global recruitment (Experiment 1), in all pigs, followed the same pattern with large values at lowest PEEP and decreasing towards zero as PEEP increased, it seemed legitimate to measure the dispersion around an exponential curve fitted to the data. Nevertheless, the initial magnitude and the decay rate differed from one pig to another (Fig. 2 left), so that appropriate normalization was done to provide an overall measure of dispersion dependent on the chosen strategy. The actual procedure was as follows. First, an exponential curve $\tilde{y}_{ps}(x) = A_{ps}\exp(-\beta_{ps}x)$ was fitted separately to each set of points $\{y_{ps}(x)\}$ representing recruitment vs. PEEP in a pig $p$ for a strategy $s$. Then, the experimental points $\{y_{ps}(x)\}$ were normalized with respect to amplitude $A_{ps}$ and decay-constant $\beta_{ps}$: $\hat{y}_{ps}(x/\beta_{ps}) = y_{ps}(x)/A_{ps}$. Subsequently, all the normalized points from the same strategy were merged together into a point set $\{\hat{y}_s\}$. Eventually, exponential fit was separately calculated for each set $\{\hat{y}_s\}$, and the corresponding coefficient of determination $\hat{R}_s^2$ was deduced; its values close to one correspond to small dispersion, as $1 - \hat{R}_s^2$ represents the fraction of variance unexplained. The strategy $s$ leading to the smallest dispersion of the experimental points in Experiment 1 was used as baseline in the comparisons with the subsequent experiments.

Regional-recruitment vs. PEEP curves were not expected to follow a predefined pattern. Indeed, depending on the region location and size, as well as on the pig, some regions (typically located in the anterior part of the chest) may already be aerated at the lowest PEEP and thus display a flat nearly-zero-recruitment curve, whereas in other (typically posterior) regions a relatively high PEEP may be necessary to counter the effect of gravity before recruitment begins, so that the curve displays a bump. Therefore, as exponential fit was not possible, dispersion of the regional-recruitment measurements (Experiments 2 and 3) was assessed only by calculating their variance ratio $F$. Additionally, consistency of the regional-recruitment calculations in these experiments was evaluated by summing up the recruitment values from all the boxes and comparing the sum with the baseline global-recruitment values from Experiment 1. To this purpose, linear regressions were calculated, where perfect consistency would be characterized by slope values and coefficients of determination $R^2$ equal to one.

Local recruitment values from Experiment 4 were overlaid, as color map, onto the original gray-level images, for visual-assessment purposes. Additionally, the sum of these values within the entire lungs was compared with the respective global-recruitment values by means of linear regressions.

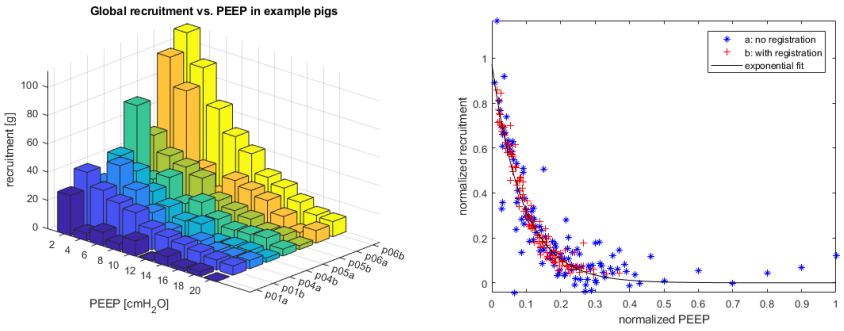


**Fig. 2** Global-recruitment values (Experiment 1) as a function of PEEP. (*left*) Examples from four pigs (p01, p04, p05, and p06) displaying, side-by-side, the results of strategies **a** and **b**. Values calculated with strategy **b** decreased more smoothly. Amplitudes and decrease rates strongly varied from one pig to another. (*right*) All results merged together after normalization and displayed along with the corresponding exponential curve for strategies **a** ($*$) and **b** ($+$), respectively. Note that the six rightmost points correspond to a pig for which the discrepancies of the values obtained with strategy **a** gave rise to an unrealistic estimate of the decay constant.

## 3 Results

In Experiment 1 (global recruitment), variance ratio $F$ was larger for strategy **b** than for strategy **a**. The respective values were: 43.4 vs. 18.8 for the factor PEEP and 13.0 vs. 6.0 for the factor pig, which means that the residual variance (dispersion) unexplained by the variations of these factors was smaller with strategy **b**.

Figure 2 displays global-recruitment values as a function of PEEP. Representative examples (Fig. 2 left), as well as the normalized points $\{\hat{y}_{s=a}\}$ and $\{\hat{y}_{s=b}\}$ (Fig. 2 right, $*$ and $+$ respectively), show that the results obtained with strategy **b** were more consistent. This visual impression was confirmed by the coefficients of determination calculated for the exponential fits: $\hat{R}^2 = 0.96$ for strategy **b** vs. $\hat{R}^2 = 0.82$ for strategy **a**. For these reasons, the results obtained with strategy **b** were considered as baseline in the subsequent comparisons. Moderate results of the linear regression between the values obtained with the two strategies, namely slope and coefficient of determination much smaller than one (see Table 2 column 1**a**), show that the recruitment values estimated by the two strategies were not very consistent with each other. On the contrary, columns 2**c** and 2**d** in Table 2 show that the sum of regional-recruitment values calculated in big boxes (Experi-

**Table 2** Linear regressions between the baseline global recruitment (Experiment 1 strategy **b**) and recruitment values calculated with other methods: global with strategy **a** (column 1**a**), sum of regional values (Experiments 2 and 3) respectively obtained with approaches **c** and **d** in big boxes (columns 2**c** and 2**d**), in medium-size boxes (columns 3**c**_m and 3**d**_m), and in small-size boxes (columns 3**c**_s and 3**d**_s), as well as sum of local values (Experiment 4) obtained using box sizes of 0.5 and 1.0 cm (columns 4_0.5 and 4_1.0).

| experiment | 1**a** | 2**c** | 2**d** | 3**c**_m | 3**d**_m | 3**c**_s | 3**d**_s | 4_0.5 | 4_1.0 |
|---|---|---|---|---|---|---|---|---|---|
| slope | 0.718 | 0.981 | 1.000 | 0.981 | 1.000 | 0.938 | 1.000 | 0.951 | 0.966 |
| $R^2$ | 0.772 | 0.998 | 1.000 | 0.998 | 1.000 | 0.955 | 1.000 | 0.879 | 0.886 |

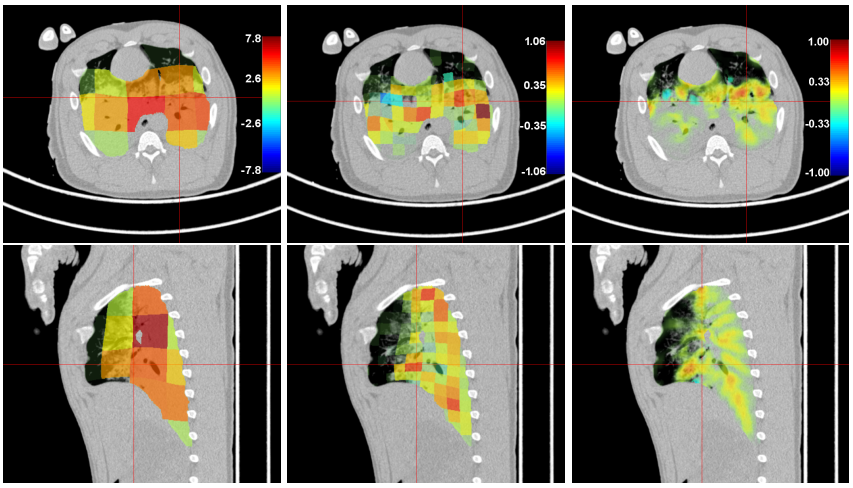


**Fig. 3** Examples of recruitment maps obtained at low PEEP (2 cm $H_2O$). Regional maps generated with medium-size (*left*) and small (*center*) boxes, respectively; the scale of recruitment is given in grams and is symmetric: deep red color corresponds to the actual maximum observed in the image, blue color represents derecruitment, if any, and green color corresponding to zero was made transparent to improve legibility. Local map (*right*) calculated using a box size of 1.0 cm. In the latter, the color scale was set between -1 and 1 regardless the actual maximum ratio $\rho$ observed within the map. Note the large size of the opacities and the absence of contrast between the lung parenchyma and the surrounding tissues in the posterior regions.

ment 2) was tightly correlated with the corresponding baseline global recruitment in each pig and at each PEEP. Representative examples (supplementary material[2], Fig. S1) show that the values obtained using warped boxes were consistently positive and predominantly decreasing when PEEP increased, while they were somewhat chaotic when the shape changes of the boxes were neglected. Variance ratios $F$ obtained in regional-recruitment quantification using big boxes (supplementary Table S1) also demonstrate that the results obtained in warped boxes were systematically better than without warping.

Variance ratios $F$ obtained using medium-size boxes (Experiment 3) were better with approach **d** in 85% of regions with respect to the factor PEEP and in 80% of regions with respect to the factor pig. Figure 3 (also see its extended version, supplementary Figure S2) displays an example of recruitment values – calculated regionally in medium-size (left) and small boxes (middle) – and superimposed as a color map onto the gray levels of the corresponding image slice. It can be seen that the boundaries of the boxes were warped based on image registration. The map gives an increasingly localized insight to the recruitment as the box size decreases, but values obtained in smaller boxes are more sensitive to registration errors (see the blue color representing negative recruitment, which is rather unlikely; also refer to supplementary material for the corresponding results of registration, shown in Figure S3 bottom, and their discussion). The sum of recruitment values calculated in these boxes remained very close to the baseline global recruitment, as illustrated by the results of linear regression (Table 2 columns 3**c**_m through 3**d**_s).

[2] `https://www.creatis.insa-lyon.fr/~orkisz/supplementary_material_1.pdf`

In the example from Figure 3, the lung volume was of 1069 ml, out of which 687 ml were non-aerated at end-exhale, and the global intratidal recruitment at end-inhale was of 112 g. The non-aerated tissues were mainly located in the dependent (posterior) regions; the largest volume (196 and 132 ml) of non-aerated tissues at end-exhale was observed in the right and left posterior big boxes located at mid-height, and the corresponding recruitment also was the greatest (21 and 24 g respectively, which makes together more than one third of the global recruitment). The two, out of 120, most-recruited (7.2 and 7.8 g) medium-size boxes also were located symmetrically, but slightly above the mid-height and not completely posterior (see supplementary Figure S2, coronal and sagittal cuts), probably because the most-dependent regions were recruited at higher PEEP. In small boxes, the maximum recruitment was of 1.1 g, which corresponds one third of the tissues contained in the box, and the locations of the most-recruited boxes were more heterogeneous – reflecting the heterogeneity of the opacities observed at this scale.

Figure 3 right (also see supplementary Figure S3 top) displays an example of local-recruitment map (Experiment 4). It shows a further increase in localization with respect to regional-recruitment maps. A supplementary video[3] displays another example of local-recruitment map at PEEP= 2 cm $H_2O$. A second video[4] and the supplementary Figure S4 show the local-recruitment changes in the same pig with PEEP value varying from 2 to 20 cm $H_2O$. Linear-regression results reported in Table 2 (columns 4_0.5 and 4_1.0) and the supplementary Figure S5 show that the sum of the local-recruitment values within the whole lungs was consistent with the baseline global-recruitment values, although the dispersion was larger than in the regional-recruitment results. Actually, the linear regression was biased by four outliers corresponding to the lowest pressures in pig 4. In the corresponding images, the extent of the opacities was particularly large (see Figure 3); therefore, both the interactive delineation of $\mathcal{L}_2$ and the automatic image registration were very difficult, which may explain the observed discrepancies. After exclusion of these four points, the coefficient of determination increased over 0.97 for both box sizes. Similarly, the sums of the local-recruitment values calculated separately for each region were consistent with the corresponding regional-recruitment values. After exclusion of the low-PEEP outliers from pig 4, $R^2$ was of 0.95 in big boxes, and of 0.81 in medium-size boxes (also see the supplementary Figures S6 and S7).

Calculating global recruitment took three minutes per image pair. In regional- and local-recruitment experiments, computational time was strongly dependent on the box size. In Experiments 2 and 3, box-size reduction increased the number of regions, and the respective processing time for big, medium-, and small-size boxes was of five minutes, ten minutes and three hours. Conversely, as local recruitment is calculated at a constant number of locations, regardless the box-size, the number of boxes remains unchanged, but a bigger size implies more operations within the box, so the increase from 0.5 to 1.0 cm increased the computational time from twenty minutes to three hours, respectively. No attempt was made to optimize the implementation and thus reduce the processing time.

[3] `https://www.creatis.insa-lyon.fr/~orkisz/pig20_moving_slice.mp4`

[4] `https://www.creatis.insa-lyon.fr/~orkisz/pig20_changing_PEEP.mp4`

## 4 Discussion

The objective of the work presented in this article was to assess regional and local lung aeration changes induced by various mechanical-ventilation settings, with particular focus on alveolar recruitment. The methods proposed in this article tackled two limitations of the previous approaches that were unable to account for non-rigid tissue motion and to display voxel-wise recruitment maps. They build on preliminary image registration devised to align the pulmonary structures and on a new computational scheme that brought the existing global/regional recruitment definitions to a voxel level. Our results confirmed the usefulness of image registration to reduce human interaction in lung segmentation, as previously suggested [8, 16], and thus improve reproducibility of global-recruitment quantification. Reproducibility of regional-recruitment assessment also was improved by aligning the tissues encompassed by the regions. The numerical values of the regional recruitment seem consistent. Bigger values were observed at locations containing a larger proportion of non-aerated voxels at end-exhale and a smaller proportion at end-inhale. These values decreased when calculated within smaller regions, but this decrease was slower than the decrement of the region size, because big regions contain heterogeneous tissues, while a small region is more likely to contain more homogeneous ones. Local-recruitment values integrated over the whole lungs were consistent with global recruitment. We illustrated the ability of the new method to highlight the regions that undergo intratidal recruitment.

These overall good results were obtained using a general-purpose registration method. Nevertheless, their detailed inspection showed some inconsistencies due to registration errors. Registration of images from subjects with ARDS is a difficult task and has been very little explored thus far. Main difficulties reside in the loss of contrasts and in dramatic density changes in recruited regions: existing methods "drag" tissues towards incorrect locations when uselessly attempting to align the boundaries of shrunken non-aerated regions. In case of slight misalignment, strong differences in density between airway wall and lumen, or between vessels and the surrounding aerated parenchyma may be interpreted as local (de-)recruitment. This effect is averaged out, and hence less perceptible, when using larger boxes. Box size is a trade-off between localization, robustness, and processing time. The latter dramatically increased with box size in the local approach. Smaller box size improved localization but resulted in larger sensitivity to alignment errors. To reduce misalignment and thereby increase the reliability of the measures thus calculated, forthcoming research should be oriented to improve the registration of the specific CT images representing ARDS.

A limitation of the work presented herein is the lack of validation against ground truth, because it does not exist and our proposal is exploratory.

Nevertheless, let us stress that local recruitment has never been calculated and displayed before, and the method proposed is an important step toward the assessment of local changes in lung aeration. Displaying such local changes may give better insight into the state of pulmonary tissues suffering from ARDS and into their response to mechanical ventilation, thus opening a path toward better-adapted patient-specific ventilator settings. The same computational scheme is potentially applicable to locally calculate aeration indexes other than recruitment, e.g., local distention. It can also be used to compute regional measures in anatomically- or functionally-meaningful regions instead of boxes.

In conclusion, our results show that automatic image registration can improve the assessment of alveolar recruitment from CT images, because it compensates tissue displacement and deformation, and that the new method proposed to assess the recruitment at voxel scale is consistent with regional and global recruitment quantification. These methods may therefore be used on data from clinical practice as far as a pair of CT scans acquired at different ventilation conditions are available for a given patient. Hence, further studies using these methods can now be foreseen to better understand the pathological mechanisms and optimize the therapy.

*Ethical approval:* This study was approved by our Institutional Review Board for the care of animal subjects (Comité d'Expérimentation Animale de l'Université Lyon 1). All procedures performed in studies involving animals were in accordance with the ethical standards of the institution at which the studies were conducted. All applicable international, national, and/or institutional guidelines for the care and use of animals were followed.

*Conflict of Interest:* The authors declare that they have no conflict of interest.

## References

1. Caironi, P., Cressoni, M., Chiumello, D., Ranieri, M., Quintel, M., Russo, S.G., Cornejo, R., Bugedo, G., Carlesso, E., Russo, R., Caspani, L., Gattinoni, L.: Lung opening and closing during ventilation of acute respiratory distress syndrome. Am J Respir Crit Care Med **181**(6), 578–586 (2010). DOI 10.1164/rccm.200905-0787OC
2. Crotti, S., Mascheroni, D., Caironi, P., Pelosi, P., Ronzoni, G., Mondino, M., Marini, J.J., Gattinoni, L.: Recruitment and derecruitment during acute respiratory failure. American Journal of Respiratory and Critical Care Medicine **164**(1), 131–140 (2001). DOI 10.1164/ajrccm.164.1.2007011
3. Fanelli, V., Vlachou, A., Ghannadian, S., Simonetti, U., Slutsky, A.S., Zhang, H.: Acute respiratory distress syndrome: new definition, current and future therapeutic options. J Thor Dis **5**(3), 326–334 (2013). DOI 10.3978/j.issn.2072-1439.2013.04.05
4. Gattinoni, L., Caironi, P., Cressoni, M., Chiumello, D., Ranieri, V.M., Quintel, M., Russo, S., Patroniti, N., Cornejo, R., Bugedo, G.: Lung recruitment in patients with the acute respiratory distress syndrome. New Engl J Med **354**(17), 1775–1786 (2006). DOI 10.1056/NEJMoa052052
5. Gattinoni, L., Pelosi, P., Crotti, S., Valenza, F.: Effects of positive end-expiratory pressure on regional distribution of tidal volume and recruitment in adult respiratory distress syndrome. Am J Respir Crit Care Med **151**(6), 1807–1814 (1995). DOI 10.1164/ajrccm.151.6.7767524
6. Klein, S., Staring, M., Murphy, K., Viergever, M., Pluim, J.: elastix: A toolbox for intensity-based medical image registration. IEEE Transactions on Medical Imaging **29**(1), 196–205 (2010)
7. Malbouisson, L.M., Muller, J.C., Constantin, J.M., Lu, Q., Puybasset, L., Rouby, J.J., the CT Scan ARDS Study Group: Computed tomography assessment of positive end-expiratory pressure-induced alveolar recruitment in patients with acute respiratory distress syndrome. Am J Respir Crit Care Med **163**(6), 1444–1450 (2001). DOI 10.1164/ajrccm.163.6.2005001
8. Morales Pinzón, A., Orkisz, M., Richard, J.C., Hernández Hoyos, M.: Lung segmentation by cascade registration. IRBM **38**, 266–280 (2017). DOI 10.1016/j.irbm.2017.07.003
9. Nieman, G.F., Satalin, J., Andrews, P., Aiash, H., Habashi, N.M., Gatto, L.A.: Personalizing mechanical ventilation according to physiologic parameters to stabilize alveoli and minimize ventilator induced lung injury (VILI). Intensive Care Med Exp **5**(1) (2017). DOI 10.1186/s40635-017-0121-x

10. Pelosi, P., Goldner, M., McKibben, A., Adams, A., Eccher, G., Caironi, P., Losappio, S., Gattinoni, L., Marini, J.J.: Recruitment and derecruitment during acute respiratory failure. an experimental study. Am J Respir Crit Care Med **164**, 122–130 (2001). DOI 10.1164/ajrccm.164.1.2007010
11. Richard, J.C., Pouzot, C., Morales Pinzón, A., Torres González, J.S., Orkisz, M., Neyran, B., Hernández Hoyos, M., Lavenne, F., Guérin, C.: Reliability of the nitrogen washin-washout technique to assess end-expiratory lung volume at variable PEEP and tidal volumes. Intensive Care Med Exp **2**(1) (2014). DOI 10.1186/2197-425X-2-10
12. Shamonin, D.P., Bron, E.E., Lelieveldt, B.P., Smits, M., Klein, S., Staring, M.: Fast parallel image registration on CPU and GPU for diagnostic classification of Alzheimer's disease. Frontiers in Neuroinformatics **7**(50), 1–15 (2014)
13. Top, A., Hamarneh, G., Abugharbieh, R.: Spotlight: Automated confidence-based user guidance for increasing efficiency in interactive 3D image segmentation. In: B. Menze, G. Langs, Z. Tu, A. Criminisi (eds.) Medical Computer Vision. Recognition Techniques and Applications in Medical Imaging, *Lecture Notes in Computer Science*, vol. 6533, pp. 204–213. Springer Berlin Heidelberg, Beijing, China (2010). DOI 10.1007/978-3-642-18421-5_20
14. Top, A., Hamarneh, G., Abugharbieh, R.: Active learning for interactive 3D image segmentation. In: G. Fichtinger, A. Martel, T. Peters (eds.) Medical Image Computing and Computer-Assisted Intervention (MICCAI), *Lecture Notes in Computer Science*, vol. 6893, pp. 603–610. Springer Berlin / Heidelberg, Toronto, Canada (2011). DOI 10.1007/978-3-642-23626-6_74
15. Vieira, S.R.R., Puybasset, L., Richecoeur, J., Lu, Q., Cluzel, P., Gusman, P.B., Coriat P. Rouby, J.J.: A lung computed tomographic assessment of positive end-expiratory pressure-induced lung overdistention. Am J Respir Crit Care Med **158**(5), 1571–1577 (1998). DOI 10.1164/ajrccm.158.5.9802101
16. Xin, Y., Song, G., Cereda, M., Kadlecek, S., Hamedani, H., Jiang, Y., Rajaei, J., Clapp, J., Profka, H., Meeder, N., Wu, J., Tustison, N.J., Gee, J.C., Rizi, R.R.: Semiautomatic segmentation of longitudinal computed tomography images in a rat model of lung injury by surfactant depletion. Journal of Applied Physiology **118**(3), 377–385 (2015). DOI 10.1152/japplphysiol.00627.2014